ACS APPLIED MATERIALS & INTERFACES

Letter

www.acsami.org

Growth of Ultrathin MoS_2 Nanosheets with Expanded Spacing of (002) Plane on Carbon Nanotubes for High-Performance Sodium-Ion Battery Anodes

Shen Zhang,[†] Xianbo Yu,[†] Hailong Yu,[†] Yujin Chen,*[,†] Peng Gao,*[,‡] Chunyan Li,*[,†] and Chunling Zhu[‡]

[†]Key Laboratory of In-Fiber Integrated Optics, Ministry of Education, and College of Science, and [‡]College of Material Science and Chemical Engineering, Harbin Engineering University, Harbin, China

Supporting Information

ABSTRACT: A hydrothermal method was developed to grow ultrathin MoS_2 nanosheets, with an expanded spacing of the (002) planes, on carbon nanotubes. When used as a sodium-ion battery anode, the composite exhibited a specific capacity of 495.9 mAh g^{-1}, and 84.8% of the initial capacity was retained after 80 cycles, even at a current density of 200 mA g^{-1}. X-ray diffraction analyses show that the sodiation/desodiation mechanismis based on a conversion reaction. The high capacity and long-term stability at a high current ate demonstrate that the composite is a very promising candidate for use as an anode material in sodium-ion batteries.

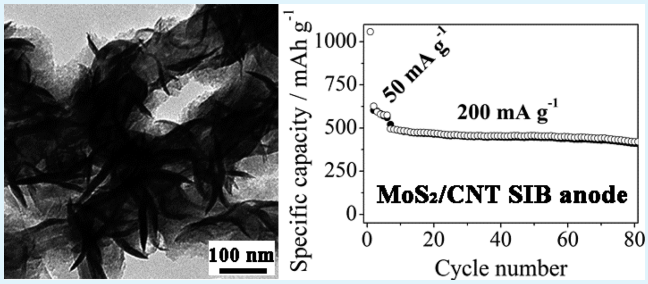

KEYWORDS: *MoS_2, carbon nanotubes, sodium-ion battery, anode, composite*

Following the development of advanced fabrication techniques, lithium-ion batteries (LIBs) have been extensively investigated as key components in portable electronic devices, hybrid electric vehicles, and aerospace technology because of their high energy density. However, the scarcity of Li resources limits the large-scale application of the LIBs. Conversely, compared with Li, Na reserves are abundant. Furthermore, sodium has a very negative redox potential of −2.71 V vs SHE and a small electrochemical equivalent of 0.86 gA h^{-1}.[1−3] Thus, sodium-ion batteries (SIBs) are very promising for large-scale energy storage applications in renewable energy and smart grid. However, Na ions have a much larger radius (ca. 1.06 Å) than Li ions (ca. 0.76 Å), leading to a strong coordination in the host lattices and slow Na ion diffusion kinetics.[1−3] Therefore, it is necessary to explore suitable host materials with sufficient Na insertion capacity, especially for anode materials. Recently, high storage sodium capacities of some metals and alloys, such as Sn and Sb, via an alloying reaction, have been demonstrated.[4−13] Komada et al. reported that Sn anodes exhibited a capacity of 500 mAh g^{-1}, which is close to the calculated value.[4] The three-dimensional tin-based anodes exhibited a capacity of 405 mAh g^{-1} after 150 cycles.[5] High capacities of Sb/C(610 mAh g^{-1})[6] and SnSb/C (544 mAh g^{-1})[7] have also been demonstrated. However, owing to the transport mechanism via an alloying reaction, the volume changes are quite large after the insertion of Na in these metals and alloys. Thus, the high rate and long cycling performances of such materials need to be further addressed. Recent studies showed that the metal oxides could also accommodate Na as the anode material.[13,14] For example, Hariharan et al. reported that Fe_3O_4, when used as the anode material in SIBs, exhibited discharge and charge capacities of 643 and 366 mAh g^{-1}, respectively.[13] Fe_2O_3/graphene composites exhibited a reversible capacity of 410 mAh g^{-1} even after 100 cycles at a current density of 100 mAh g^{-1}.[14] However, the long life of the metal oxide based anodes at a high current density is still insufficient. Very recently, SnS based composites, when used as SIB anode materials, exhibited very high electrochemical performances resulting from small structural changes of SnS during the sodiation/desodiation process.[15]

MoS_2 is a typical layered structure and the spacing between the neighboring layers for bulk MoS_2 is about 0.615 nm, which is significantly larger than that of graphite (0.335 nm). Furthermore, the van der Waals forces between the layers are relatively weak. As a consequence, MoS_2 may be successfully used as anode material in SIBs, although it has been reported having a very weak Na storage capability.[16] Recently, David et al. fabricated MoS_2/graphene composite paper as a self-standing flexible electrode in SIBs.[17] The electrode showed a good Na cycling ability with a stable charge capacity of approximately 230 mAh g^{-1}, with respect to the total weight of the electrode, reaching a 99% Coulombic efficiency. This result indicates that MoS_2-based nanocomposites can be used as anode materials in high-performance SIBs if their structures are rationally designed.[18]

Some methods have been developed to grow MoS_2 nanosheets on carbon nanotubes or graphene sheets. However,

Received: September 9, 2014
Accepted: December 5, 2014
Published: December 5, 2014

the spacing of the (002) crystal planes was not expanded efficiently.[19] Herein we develop a hydrothermal method to grow ultrathin MoS_2 nanosheets with an expanded spacing of the (002) crystal planes on the surfaces of carbon nanotubes (CNTs). When adopted as anode material for SIBs, this interesting three-dimensional (3D) hierarchical composite delivers a reversible specific capacity of 504.6 mAh g^{-1}at a current rate of 50 mA g^{-1} over 100 cycles, and a specific capacity of 495.9 mAh g^{-1}at a current rate of 200 mA g^{-1}, retaining 84.8% of the initial capacity after 80 cycles. The high capacity and long-term stability at a high current rate indicate that the composite is very promising for applications as SIB anode material.

The 3D MoS_2 nanosheet/CNTs (MSCNTs) were synthesized by a hydrothermal method (Supporting Information). Figure 1 shows the X-ray diffraction (XRD) pattern of the product. The diffraction peak at $2\theta = 25.9°$ corresponds to the (002) plane of the hexagonal graphite and indicates that the CNTs are present in the final product. The diffraction peaks at $2\theta = 32.5°$, 35.4°, 42.7°, and 57.0° can be indexed to the (100), (102), (006), and (110) planes of the hexagonal MoS_2 (JCPDs card number 37−1492). Two additional peaks at $2\theta = 9.09°$ and 18.2° are clearly observed in the pattern. Using the Bragg equation, their lattice spacings (d) are estimated to be 9.68 and 4.86 Å, respectively. The dual relationship between the d spacings clearly demonstrates the formation of a new lamellar structure with an enlarged interlayer spacing compared with that of the hexagonal MoS_2 (6.15 Å), which is similar to previous results.[20] Therefore, the XRD patterns show that the final product is composed of MoS_2 with an increased spacing of the (002) planes and carbon nanotubes. The expanded spacing of the MoS_2 (002) plane resulted from the synthesis conditions.[21] The spacing usually increased in the alkali solution. In addition, the environmental temperature had also a critical effect. As previously reported, at temperatures higher than 220 °C, the spacing of the (002) plane of MoS_2 could not be expanded.[20] In this work, both the alkali environment and the low temperature (200 °C) caused the expansion of the (002) plane of MoS_2.

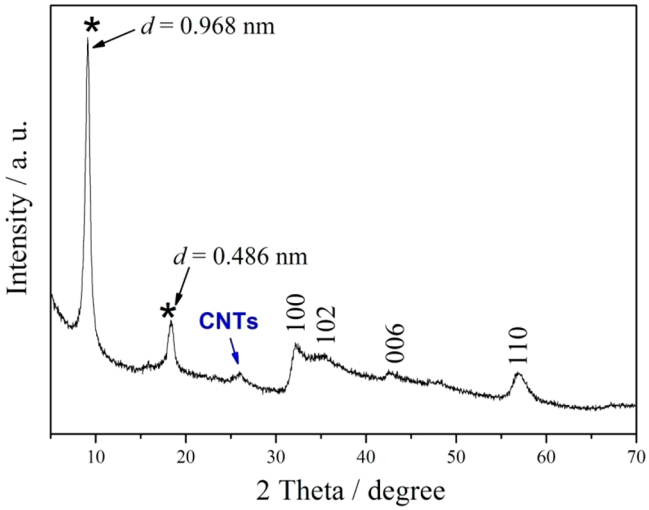

Figure 1. XRD pattern of MSCNTs.

The morphology and structure of the 3D MSCNTs were further characterized by scanning electron microscopy (SEM) and transmission electron microscopy (TEM). As shown in Figure 2a-b, ultrathin MoS_2 nanosheets were grown on the surface of the CNTs. However, without CNTs, only MoS_2 spheres were obtained (see Figure S1 in the Supporting Information). The energy-dispersive spectroscopy (EDS) spectrum (see Figure S2 in the Supporting Information) shows that the composite comprises Mo, S, and C elements. The magnified TEM images (Figure 2c, d) indicate that the basal plane of the majority of the MoS_2 nanosheets is placed vertically with respect to the external wall of the CNTs (marked by a white arrow in Figure 2d). Figure 2e shows that the thickness of most of the MoS_2 nanosheets is less than 10 nm, and decreases below 4 nm for some of them (marked by white

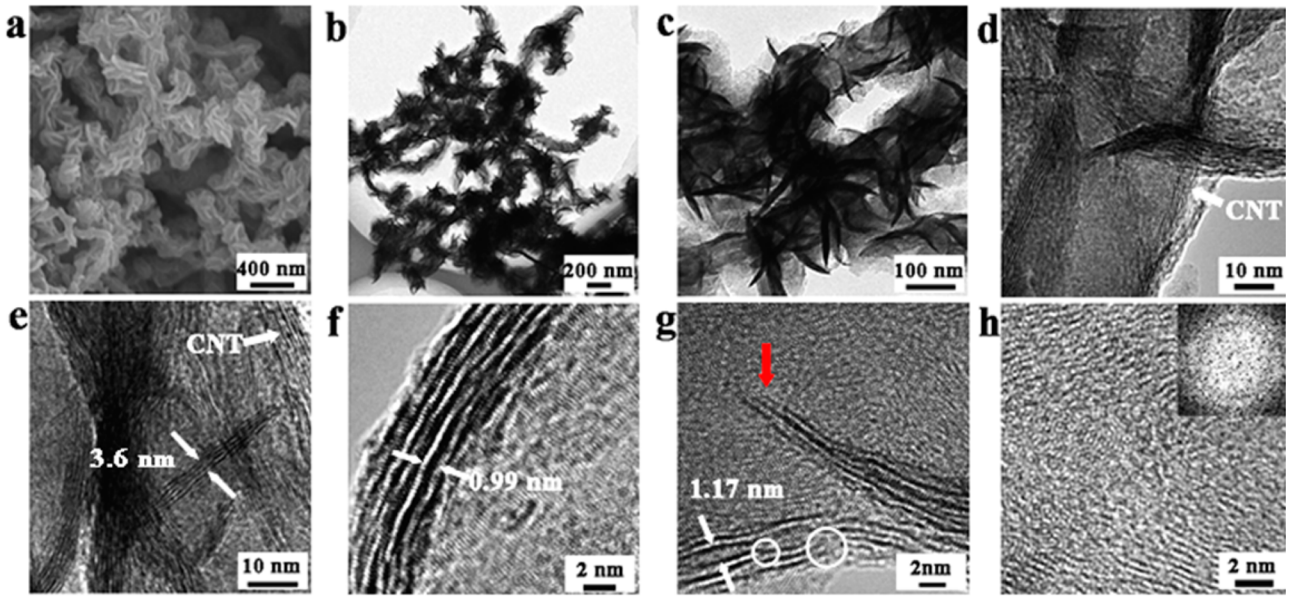

Figure 2. Structrual characterization of MSCNTs. (a) SEM, (b) low-resolution TEM, (c−e) magnified TEM, and (f−h) HRTEM images. The inset in h showing a FFT image.

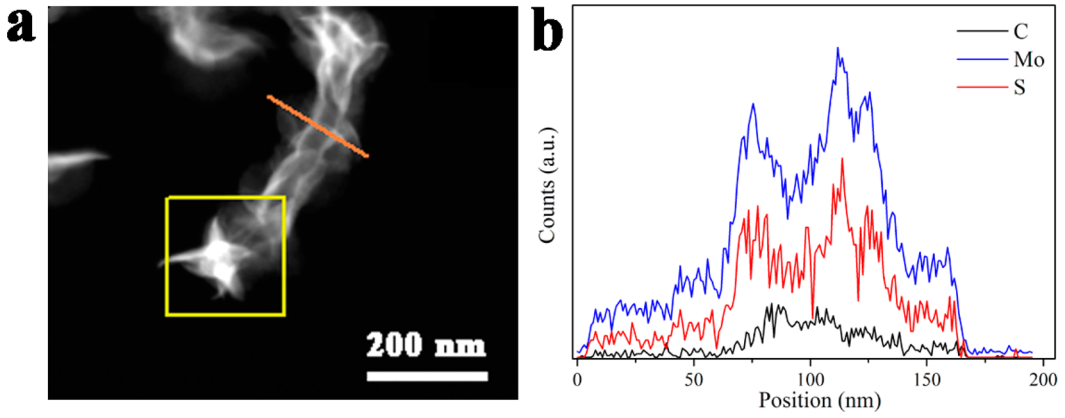

Figure 3. (a) ADF STEM image, and (b) EDX elemental scanning mappings of 3D MSCNTs.

arrows). Furthermore, the thickness of most of the MoS_2 nanosheets at both ends, marked by a red arrow in Figure 2g, is less than 2 nm. The discontinued fringes at the edges, observed in the high-resolution (HR) TEM images (marked with white circles in Figure 2f, g), indicate that rich defects, presumably induced by the enlarged spacing of the (002) crystal planes,[20] exist in the MoS_2 nanosheets. As shown in Figure 2g, h, the interlayer distance is approximately 0.99 nm even in the middle region of the edges, and increases up to 1.1 nm at the ends of edges, consistently with the XRD measurements. The expanded distance of the (002) crystal planes facilitates the Na ion storage in the ultrathin MoS_2 nanosheets. Moreover, the atomic arrangement on the basal surface appears highly disordered and even short-range ordering of the nanodomains is not present (Figure 2h), suggesting very poor crystallinity of the basal surfaces of the MoS_2 nanosheets. Only one closed diffraction ring can be observed in the fast Fourier transform (FFT) applied to the HRTEM image (inset in Figure 2h), further confirming the strongly disordered arrangement of the nanodomains. The rich defects and poor crystallinity of the basal surfaces may promote an improvement of the electrochemical performance of MoS_2.[20] The 3D MSCNTs contain about 76.7 wt % of MoS_2, determined with a CS-206 infrared carbon and sulfur analyzer.

To further ascertain the distribution of the elements in the 3D MSCNTs, annular dark-field (ADF) scanning transmission electron microscopy (STEM, Figure 3a) and the corresponding energy dispersive X-ray spectrometry (EDX) elemental scanning mappings (Figure 3b) were carried out. The measurements reveal that the Mo and S elements mainly distribute in the external region, whereas C is more present in the inner part.

The surface electronic state and composition of the 3D MSCNTs were investigated by XPS analysis. The XPS survey spectrum indicates that the composite contains C, Mo, S, and O elements, as shown in Figure S3a (Supporting Information). In the high-resolution S 2p spectra shown in Figure S3b (Supporting Information), the peaks observed at 161.7 and 162.9 eV correspond to S^{2-} $2p_{3/2}$ and S^{2-} $2p_{1/2}$, respectively. The intensity ratio of the characteristic peaks is approximately 2:1 and their separation energy is ca. 1.2 eV, which is typical for S^{2-} species. Figure S3c (Supporting Information) shows a high-resolution spectrum in the binding energy range of 223−240 eV. The peaks at 228.8 and 231.9 eV correspond to the Mo^{4+} $3d_{5/2}$ and Mo^{4+} $3d_{3/2}$ components in MoS_2, respectively. The $3d_{3/2}$ and $3d_{5/2}$ peaks have separation energies close to 3.1 eV, characteristic of the Mo species.[22,23] The peak at around 235.8 eV, assigned to Mo^{6+}, is negligible, suggesting that the amount of MoO_3 is minimal in the product. Figure S3d (Supporting Information) shows the standard carbon peak at 284.6 eV, with the asymmetric peak indicating that C−O and C═O groups exist on the surfaces of the CNTs.

The presence of MoS_2 and carbon nanotubes in the 3D MSCNTs is further confirmed by the Raman measurements (Figure S4, Supporting Information). The Raman peaks at 374 and 401 cm^{-1}, ascribed to E^1_{2g} and A_{1g}, respectively, are characteristic peaks of the hexagonal MoS_2.[24,25] The Raman peaks at around 1352.6 and 1572.6 cm^{-1}, corresponding to D-band and G-band, respectively, belong to the carbon nanotubes. The intensity ratio of the D-band and G-band is significantly below 1.0, indicating that the carbon nanotubes have a high degree of graphitization.[26] Compared with CNTs, the intensity of the D- and G-bands in the MSCNTs decreases considerably because of the dense MoS_2 nanosheets grown on the surface of the CNTs. Notably, the additional amount of CNTs plays an important role in the successful synthesis of uniform MSCNTs. When the amount of CNTs decreased below 1 mg (Figure S5a, Supporting Information), there were large MoS_2 spheres in the final product; however, when the amount of CNTs increased above 5 mg (Figure S5b, Supporting Information), most of the CNTs were not coated by MoS_2 nanosheets.

The 3D hierarchical nanostructures, composed of ultrathin MoS_2 nanosheets with an expanded spacing of the (002) crystal plane grown vertically on the surface of the CNTs, provide shorter Na-ion diffusion channels and high conductivity for Na-ion storage, and may therefore exhibit good electrochemical performances when used as anode materials in SIBs. The electrochemical properties of MSCNTs were first evaluated by cyclic voltammograms (CV). As shown in Figure S6, three reduction peaks at 1.3, 0.66, and 0.005 V and the oxidation peaks at 2.2, 1.7, and 0.5 V were observed in the first cycle. In the second cycle, the reduction peaks at 1.3 and 0.66 V shift to higher potential of 1.5 and 0.77 V, respectively. At the same time, the intensity of the peak at 0.77 V decreases after the second cycle, indicating the solid electrolyte interphase (SEI) layer is formed on the MSCNT surface. SEI layer leads to irreversible capacity loss in the first cycle. After the second cycle, the reduction and oxidation peaks have almost not changed in the intensity and position, indicating a good cycling stability of MSCNTs. During the reduction process, the peak at around 1.5 V corresponds to the intercalation of Na ions into the interlayer of MoS_2[17,27]

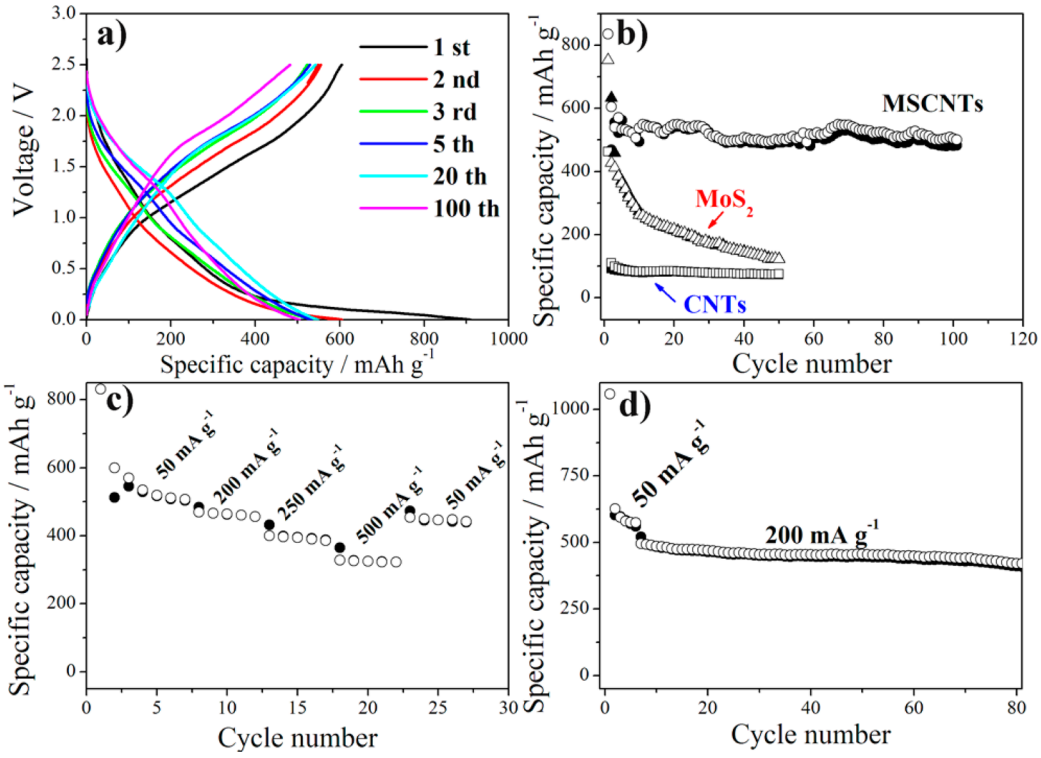

Figure 4. Electrochemical performances of different samples. (a) typical voltage versus specific capacity profiles of MSCNTs for the different discharge/charge cycles; (b) cycling performances of MSCNTs, MoS_2 spheres, and CNTs at a current density of 50 mAh g^{-1}; (c) rate performances of MSCNTs; and (d) stability of MSCNTs at a current density of 200 mAh g^{-1}.

$$MoS_2 + yNa^+ + ye^- \rightarrow Na_yMoS_2 \quad (1)$$

The peak at around 0.66 V indicates that the conversion reaction occurs.

$$Na_yMoS_2 + (4 - y)Na^+ + (4 - y)e^- \rightarrow 2NaS_2 + Mo \quad (2)$$

In addition, the peak at low potential of around 0.005 V is attributed to the Na ion adsorption on the interface between NaS_2 and Mo.[17,27]

The electrochemical performance of MSCNTs, MoS_2 spheres obtained without CNTs, and CNTs was further evaluated using coin cells with sodium metal as a counter electrode. Figure 4a shows the voltage−capacity curves at a low current density of 50 mA g^{-1}. The initial discharge curve shows three plateaus at 1.5−0.9, 0.9−0.3, and 0.3−0 V, consistent with the analyses of CV. Although the width of the plateau at a low potential region is gradually shorten after the initial cycle, the other two plateaus still presented, which suggest highly reversible Na ion storage in MSCNTs. The discharge capacities in the first, second, and third cycles are 835.6, 604.7, and 539.9 mAh g^{-1}, respectively. Even after 100 cycles, both the discharge and the charge capacities of the 3D MSCNTs are stable at ca.504.6 mAh g^{-1}, delivering 93.5% of the third cycle capacity. The Columbic efficiency is 77.4% after the first charging and discharging processes, and remains in the range of 91.6−100% during the successive 100 cycles. The reversible capacity stabilizes in the range of 539.9−504.6 mAh g^{-1} with an initial capacity retention of 89.3% during the following 100 cycles (Figure 4b), suggesting that the 3D MSCNTs have a good cycling performance at a low current rate of 50 mAh g^{-1}. Compared with the carbon nanotubes and MoS_2 flowers, the 3D MSCNTs exhibit excellent electrochemical performances. As shown in Figure 4b, the reversible discharge capacities of the MoS_2 flowers and carbon nanotubes are 427.4 and 97.3 mAh g^{-1}, respectively, significantly lower than that of the 3D MSCNTs. Furthermore, after 50 cycles their reversible capacities are only 28 and 64% of the initial capacities. Thus, the incorporation of carbon nanotubes remarkably enhances the electrochemical properties of the MoS_2 nanosheets. More importantly, compared with other MoS_2 samples, the 3D MoS_2 nanosheet/CNTs exhibit enhanced rate capabilities.[17,18] For example, the discharging capacity of the MoS_2/graphene paper at a current density of 25 mA g^{-1} is equal to 250 mAh g^{-1}, whereas the capacity of the 3D MSCNTs increase up to 504.6 mAh g^{-1} at a current density of 50 mA g^{-1} even after 100 cycles (Table S1, Supporting Information).[17]

Because of the unique 3D architectures, the MSCNTs also exhibit very good high-rate electrochemical performances. As shown in Figure 4c, the reversible capacity of the 3D MSCNTs increases up to 328.4 mAh g^{-1} even at a high current density of 500 mA g^{-1}, and considerably higher than that of the carbon nanotubes and MoS_2 spheres (Figure S7, Supporting Information). Moreover, after a highly rapid charging/discharging process, the discharge capacity of the 3D MSCNTs can recover 84.2% of the initial capacity at a current density of 50 mA g^{-1}, suggesting an excellent rate cycling stability of the anodes. The long-term stability of the electrochemical performance of the 3D MSCNTs was further tested at a current density of 200 mA g^{-1}. Figure 4d shows the cycling behavior of another SIB anode, initially at 50 mA g^{-1} for several cycles, and then at 200 mA g^{-1} for 80 cycles. The MSCNTs clearly exhibit a specific capacity of 495.9 mAh g^{-1} retaining 84.8% of the initial capacity after 80 cycles at the current rate. Moreover, the Coulombic efficiency is in the range of 96−100% (Figure S8, Supporting Information). Table S1 (Supporting Information)

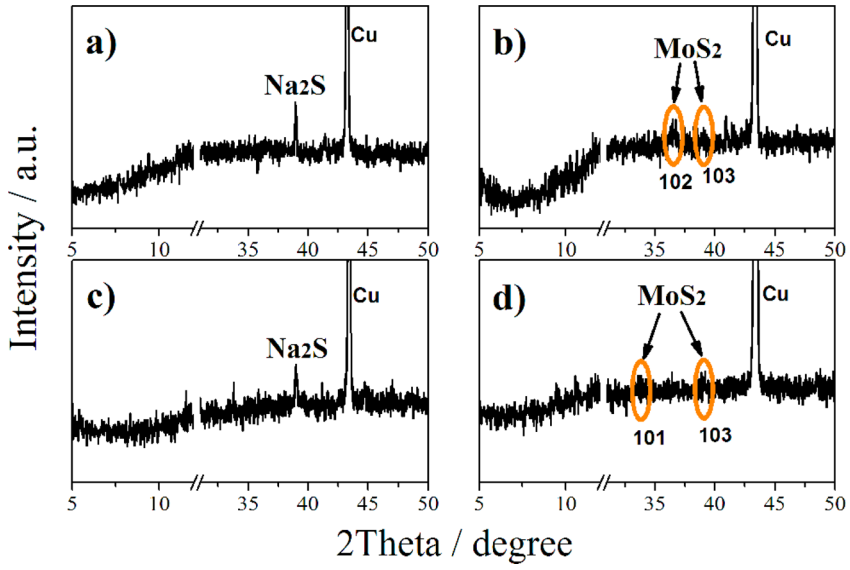

Figure 5. Ex situ XRD patterns of MSCNT electrodes at different states after different charged/discharged cycles. (a) The first fully discharged process, (b) the first fully charged process, (c) the fully discharged process after 100 cycles, and (d) the fully charged process after 100 cycles.

compares our results with the state of the art results reported in previous research on SIB anode materials. It is found that the rate-performance of our prepared 3D MSCNTs is considerably higher than those of most anode materials for SIBs.[5,10,28]

Considering the structural characteristics of the 3D MSCNTs, the excellent electrochemical performances could be ascribed to the following factors. (i) The thickness of the majority of the MoS_2 nanosheets is less than 10 nm (Figure 2d–f), providing a short pathway for the Na ion diffusion and a low activation energy for the Na ion intercalation reaction. (ii) The very low conductivity between two adjacent van der Waals bonded S–Mo–S sheets of the bulk MoS_2 significantly limits the rate of the Na ion intercalation.[28] The conductivity of the MoS_2 nanosheets is greatly improved as they are grown vertically on the surfaces of the CNTs. The enhanced conductivity is attributed to the rapid electron transport during the Na insertion/extraction reaction. An electrochemical impedance spectroscopy (EIS) analysis of the MoS_2 spheres and 3D MSCNT electrodes was conducted to investigate the improved conductivity. Figure S9 (Supporting Information) shows both Nyquist plots, consisting of one semicircle in the high-frequency region and a straight line in the low-frequency region. The depressed semicircle in the high-frequency region is attributed to a charge-transfer process. The diameter of the semicircle in the 3D MSCTNs plot is smaller than that in the spheres plot, indicating that the charge-transfer resistance at the electrode/electrolyte interface of the 3D MSCTNs is significantly lower than that of the MoS_2 nanospheres. (iii) The lattice distance of the (002) planes of the MoS_2 nanosheets increased up to 0.968–1.10 nm. The increased spacing facilitates the Na ion insertion/extraction compared with the bulk MoS_2. (iv) As the MoS_2 nanosheets are grown on the surfaces of the CNTs, there is a void space, among neighboring nanosheets, that facilitates an efficient contact of the electrolyte with the active materials. (v) The high mechanical strength enables the CNTs to withstand the stress and volume variation accompanying the Na charging/discharging process.

To reveal the charge/discharge mechanism of the 3D MSCNTs, ex situ XRD analyses were carried out to determine the compositional changes of fully discharged and charged electrodes after the first cycle and after 100 cycles. Before the measurements, the electrodes were immersed in dimethyl carbonate to remove $NaPF_6$. In all the XRD patterns, the strong peaks located at $2\theta = 38.9°$ are attributed to the copper current collector. After the first discharge (Figure 5a), a peak located at $2\theta = 38.9°$, indexed to the (220) plane of Na_2S (JCPDs card number 03–0933), can be observed, whereas the MoS_2 peaks disappear. This result suggests that MoS_2 is converted to Na_2S after a fully discharged process. As shown in Figure 5b, after the first fully charged process, the diffraction peak from Na_2S disappears. However, two diffraction peaks corresponding to (102) and (103) crystal planes of MoS_2 (marked with blue circles in Figure 5b), respectively, are emerged out, indicating that Na_2S is converted to MoS_2 after a fully charged process. It should be noted that the diffraction peaks corresponding to (002) crystal plane of MoS_2 is not observed. It may be attributed to further expanded *d*-spacing of (002) crystal plane of MoS_2 due to Na ion intercalation into MoS_2 interlayer or the change in the structure from a few layered MoS_2 to single-layered MoS_2.[27] The phenomenon is common found in the delithiation process of MoS_2[29] Similar results can be obtained for the electrodes after 100 cycles, as shown in Figure 5c-d. The different diffraction peaks in the different cycles (Figure 5b and Figure 5d) may be attributed to the change in the crystal structure of MoS_2, which has been also found in the desodiation process of bulk MoS_2.[27] The XRD results are consistent with the analyses of CV, and thereby the sodiation/desodiation mechanism of the MSCNTs appears to be based on a conversion reaction, i.e., $MoS_2 + 4Na^+ + 4e^- \rightarrow 2Na_2S + Mo$.[17,18]

In summary, we developed a hydrothermal method to grow ultrathin MoS_2 nanosheets on the surfaces of carbon nanotubes. The thickness of the MoS_2nanosheets is less than 10 nm, and the interlayer spacing is increased to 0.968–1.10 nm. Because of the small size and expanded interlayer spacing of MoS_2, as well as to a high conductivity, the MoS_2/CNTs exhibit excellent electrochemical performance as they serve as anode materials for SIBs. The MoS_2/CNTs deliver a reversible specific capacity of 504.6 mAh g^{-1} at a current rate of 50 mA g^{-1} over 100 cycles, and a specific capacity of 495.9 mAh g^{-1} at a current rate

of 200 mA g^{-1}, retaining 84.8% of their initial capacity after 80 cycles. The high capacity and long-term stability at a high current rate indicate that the MoS_2/CNTs are very promising for applications in SIB anode materials.

■ ASSOCIATED CONTENT

Supporting Information

EDS, Raman, and XPS spectra of 3D MSCNTs, SEM image of MoS_2 spheres, rate performances of CNTs and MoS_2 spheres, Columbic efficiency of MSCNTs at 200 mAh g^{-1}, and CV curves of 3D MSCNTs, and ESI spectra of 3D MSCNTs and MoS_2 spheres. This material is available free of charge via the Internet at http://pubs.acs.org/.

■ AUTHOR INFORMATION

Corresponding Authors

*E-mail: chenyujin@hrbeu.edu.cn.
*E-mail: gaopeng@hrbeu.edu.cn.
*E-mail: chunyanli@hrbeu.edu.cn.

Notes

The authors declare no competing financial interest.

■ ACKNOWLEDGMENTS

We thank the National Natural Science Foundation of China (Grant Nos. 51272050), the Innovation Foundation of Harbin City (2012RFXXG096), and the 111 project (B13015) of Ministry Education of China to the Harbin Engineering University.

■ REFERENCES

(1) Pan, H.; Hu, Y.-S.; Chen, L. Room-Temperature Stationary Sodium-Ion Batteries for Large-Scale Electric Energy Storage. *Energy Environ. Sci.* **2013**, *6*, 2338−2360.

(2) Slater, M. D.; Kim, D.; Lee, E.; Johnson, C. S. Sodium-Ion Batteries. *Adv. Funct. Mater.* **2013**, *23*, 947−958.

(3) Kim, S.-W.; Seo, D.-H.; Ma, X.; Ceder, G.; Kang, K. Electrode Materials for Rechargeable Sodium-Ion Batteries: Potential Alternatives to Current Lithium-Ion Batteries. *Adv. Energy Mater.* **2012**, *2*, 710−721.

(4) Komaba, S.; Matsuura, Y.; Ishikawa, T.; Yabuuchi, N.; Murata, W.; Kuze, S. Redox Reaction of Sn-Polyacrylate Electrodes in Aprotic Na Cell. *Electrochem. Commun.* **2012**, *21*, 65−68.

(5) Liu, Y.; Xu, Y.; Zhu, Y.; Culver, J. N.; Lundgren, C. A.; Xu, K.; Wang, C. Tin-Coated Viral Nanoforests as Sodium-Ion Battery Anodes. *ASC Nano* **2013**, *7*, 3627−3634.

(6) Qian, J.; Chen, Y.; Wu, L.; Cao, Y.; Ai, X.; Yang, H. High Capacity Na-Storage and Superior Cyclability of Nanocomposite Sb/C Anode for Na-Ion Batteries. *Chem. Commun.* **2012**, *48*, 7070−7072.

(7) Xiao, L.; Cao, Y.; Xiao, J.; Wang, W.; Kovarik, L.; Nieand, Z.; Liu, J. High Capacity, Reversible Alloying Reactions in SnSb/C Nanocomposites for Na-Ion Battery Applications. *Chem. Commun.* **2012**, *48*, 3321−3323.

(8) Ellis, L. D.; Hatchard, T. D.; Obrovac, M. N. Reversible Insertion of Sodium in Tin. *J. Electrochem. Soc.* **2012**, *159*, A1801−A1805.

(9) Darwiche, A.; Marino, C.; Sougrati, M. T.; Fraisse, B.; Stievano, L.; Monconduit, L. Better Cycling Performances of Bulk Sb in Na-Ion Batteries Compared to Li-Ion Systems: An Unexpected Electrochemical Mechanism. *J. Am. Chem. Soc.* **2012**, *134*, 20805−20811.

(10) Xu, Y.; Zhu, Y.; Liu, Y.; Wang, C. Electrochemical Performance of Porous Carbon/Tin Composite Anodes for Sodium-Ion and Lithium-Ion Batteries. *Adv. Energy Mater.* **2013**, *3*, 128−133.

(11) Zhu, H.; Jia, Z.; Chen, Y.; Weadock, N.; Wan, J.; Vaaland, O.; Han, X.; Li, T.; Hu, L. Tin Anode for Sodium-Ion Batteries Using Natural Wood Fiber as a Mechanical Buffer and Electrolyte Reservoir. *Nano Lett.* **2013**, *13*, 3093−3100.

(12) Darwiche, A.; Sougrati, M. T.; Fraisse, B.; Stievano, L.; Monconduit, L. Facile Synthesis and Long Cycle Life of SnSb as Negative Electrode Material for Na-Ion Batteries. *Electrochem. Commun.* **2013**, *32*, 18−21.

(13) Hariharan, S.; Saravanan, K.; Ramar, V.; Balaya, P. A Rationally Designed Dual Role Anode Material for Lithium-Ion and Sodium-Ion Batteries: Case Study of Eco-Friendly Fe_3O_4. *Phys. Chem. Chem. Phys.* **2013**, *15*, 2945−2953.

(14) Jian, Z.; Zhao, B.; Liu, P.; Li, F.; Zheng, M.; Chen, M.; Shi, Y.; Zhou, H. Fe_2O_3 Nanocrystals Anchored onto Graphene Nanosheets as the Anode Material for Low-Cost Sodium-Ion Batteries. *Chem. Commun.* **2014**, *50*, 1215−1217.

(15) Zhou, T. F.; Pang, W. K.; Zhang, C. F.; Yang, J. P.; Chen, Z. X.; Liu, H. K.; Guo, Z. P. Enhanced Sodium-Ion Battery Performance by Structural Phase Transition from Two-Dimensional Hexagonal-SnS_2 to Orthorhombic-SnS. *ACS Nano* **2014**, *8*, 8323−8333.

(16) Whittingham, M. S. Chemistry of Intercalation Compounds: Metal Guests in Chalcogenide Hosts. *Prog. Solid State Chem.* **1978**, *12*, 41−99.

(17) David, L.; Bhandavat, R.; Singh, G. MoS_2/Graphene Composite Paper for Sodium-Ion Battery Electrodes. *ACS Nano* **2014**, *8*, 1759−1770.

(18) Ryu, W.-H.; Jung, J.-W.; Park, K.; Kim, S.-J.; Kim, I.-D. Vine-like MoS_2 Anode Materials Self-Assembled from 1-D Nanofibers for High Capacity Sodium Rechargeable Batteries. *Nanoscale* **2014**, *6*, 10975−10981.

(19) Shi, Y.; Wang, Y.; Wong, J. I.; Tan, A. Y. S.; Hsu, C.-L.; Li, L.-J.; Lu, Y.-C.; Yang, H. Y. Self-Assembly of Hierarchical MoSx/CNT Nanocomposites (2 < x<3): Towards High Performance Anode Materials for Lithium Ion Batteries. *Sci. Rep.* **2013**, *3*, 2169.

(20) Xie, J.; Zhang, J.; Li, S.; Grote, F.; Zhang, X.; Zhang, H.; Wang, R.; Lei, Y.; Pan, B.; Xie, Y. Controllable Disorder Engineering in Oxygen-Incorporated MoS_2 Ultrathin Nanosheets for Efficient Hydrogen Evolution. *J. Am. Chem. Soc.* **2013**, *135*, 17881−17888.

(21) Bang, G. S.; Nam, K. W.; Kim, J. Y.; Shin, J.; Choi, J. W.; Choi, S. Y. Effective Liquid-Phase Exfoliation and Sodium Ion Battery Application of MoS_2 Nanosheets. *ACS Appl. Mater. Interfaces* **2014**, *6*, 7084−7089.

(22) Chang, K.; Chen, W.; Ma, L.; Li, H.; Li, H.; Huang, F.; Xu, Z.; Zhang, Q.; Lee, J.-Y. Graphene-like MoS_2/Amorphous Carbon Composites with High Capacity and Excellent Stability as Anode Materials for Lithium Ion Batteries. *J. Mater. Chem.* **2011**, *21*, 6251−6257.

(23) Kibsgaard, J.; Chen, Z.; Reinecke, B. N.; Jaramillo, T. F. Engineering the Surface Structure of MoS_2 to Preferentially Expose Active Edge Sites for Electrocatalysis. *Nat. Mater.* **2012**, *11*, 963−969.

(24) Wieting, T. J.; Verble, J. L. Infrared and Raman Studies of Long-Wavelength Optical Phonons in Hexagonal MoS_2. *Phys. Rev. B* **1971**, *3*, 4286−4292.

(25) Frey, G. L.; Tenne, R. Raman and Resonance Raman Investigation of MoS_2 Nanoparticles. *Phys. Rev. B* **1999**, *60*, 2883−2892.

(26) Eklund, P. C.; Holden, J. M.; Jishi, R. A. Vibrational Modes of Carbon Nanotubes; Spectroscopy and Theory. *Carbon* **1995**, *33*, 959−972.

(27) Park, J.; Kim, J. S.; Park, J. W.; Nam, T. H.; Kim, K. W.; Ahn, J. H.; Wang, G.; Ahn, H. J. Discharge Mechanism of MoS_2 for Sodium Ion Battery: Electrochemical Measurements and Characterization. *Electrochim. Acta* **2013**, *92*, 427−432.

(28) Tributsch, H. Layer-Type Transition Metal Dichalcogenides−a New Class of Electrodes for Electrochemical Solar Cells. *Berich. Bunsen Gesell.* **1977**, *81*, 361−369.

(29) Zeng, Z.; Yin, Z.; Huang, X.; Li, H.; He, Q.; Lu, G.; Boey, F.; Zhang, H. Single-Layer Semiconducting Nanosheets: High-Yield Preparation and Device Fabrication. *Angew. Chem., Int. Ed.* **2011**, *50*, 11093−11097.